ACS NANO

www.acsnano.org

ARTICLE

Antibody-Free Glycogen Nanoparticles Engage Human Immune T Cells for Intracellular Delivery of Small Drugs or mRNA

Soraia Fernandes, Miriam Quattrociocchi, Marco Cassani, Giulio Savazzi, Darryl Johnson, Giancarlo Forte, Frank Caruso,* and Francesca Cavalieri*

Cite This: *ACS Nano* 2024, 18, 28910−28923

Read Online

ACCESS | Metrics & More | Article Recommendations | Supporting Information

ABSTRACT: T cells play a major role in immune defense against viral infections and diseases such as cancer. Accordingly, developing nanoparticle (NP) systems to effectively deliver therapeutics to T cells is of interest. However, NP-mediated delivery of drugs to T cells is challenging because of the nonphagocytic nature of T cells. To engage T cells and induce cellular internalization, NPs are typically decorated with specific receptor-targeting antibodies, often using laborious and costly procedures. Herein, we report that natural glycogen NPs (i.e., nanosugars) with different sizes (20−80 nm) and surface charges (neutral and positively charged) engage Jurkat T cells, undergo intracellular trafficking, and release encapsulated drug without the use of receptor-targeting antibodies. Specifically, glycogen−resveratrol constructs are employed to reactivate HIV-1 latently infected Jurkat T cells (J-Lat A2) and trigger proviral expression. Both neutral and positively charged glycogen NPs engage with J-Lat A2 cells. Large (84 ± 29 nm) and positively charged (23 ± 5 mV) NPs, denoted phytoglycogen-ethylenediamine (PG_{EDA}) NPs, readily associate with the cell membrane and are internalized (60%) in J-Lat A2 cells but remain confined in the endocytic vesicles, with moderate reactivation of latent HIV-1 (4.7 ± 0.5%). Conversely, small (21 ± 5 nm) and positively charged (10 ± 6 mV) NPs, bovine glycogen-EDA (BG_{EDA}) NPs, associate slowly with T cells but show nearly 100% internalization and efficient endosomal escape properties, resulting in 1.5-fold higher reactivation of latent HIV-1 in T cells. PG_{EDA} NPs and BG_{EDA} NPs are also internalized by primary human T cells (>90% cell association) and enable the transfection of mRNA, with BG_{EDA} NPs showing a 2-fold higher transfection than PG_{EDA} NPs. This work highlights the potential of BG_{EDA} NPs for the effective intracellular delivery of small-molecule drugs and mRNA in T cells.

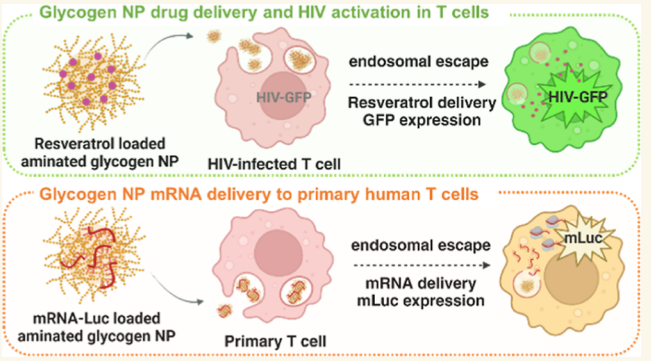

KEYWORDS: *glycogen nanoparticles, resveratrol, human immune T cells, endosomal escape, mRNA delivery*

Glycogen is a naturally occurring dendrimer-like polysaccharide composed of repeating units of glucose connected by linear α-D-(1−4) glycosidic linkages with α-D-(1−6) branching.[1] It is considered a biological nanoparticle (NP)—"nanosugar"—with size ranging from 20 to 80 nm that is formed by nature through a bottom-up approach.[1,2] Unlike other polysaccharides and oligosaccharides, such as starch,[3,4] dextran,[5,6] cellulose,[7,8] chitosan,[9,10] hyaluronic acid,[11−13] and cyclodextrin,[14−16] that have been extensively investigated in the last decades as drug delivery systems, glycogen NPs have only recently emerged as a versatile platform for drug delivery.[2] Glycogen NPs have been employed as a carrier for in vitro and in vivo delivery of poorly water-soluble small molecules, including curcumin,[17] quercetin,[18] lutein,[19] doxorubicin,[20,21] and resveratrol (RV),[22] as well as large therapeutic biomolecules such as small-interfering RNA,[23−25] plasmid DNA,[26] and insulin.[27] Owing to their dendrimer-like structure, glycogen NPs have shown many advantageous properties compared with other natural and synthetic polymer NPs, including high solubility, high colloidal stability in serum, lack of immunogenicity, tunable degradability, and multivalent binding properties.[28] We have recently demonstrated that subcutaneously injected glycogen NPs

Received: July 9, 2024
Revised: September 26, 2024
Accepted: October 2, 2024
Published: October 11, 2024

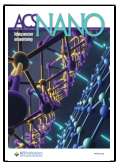

https://doi.org/10.1021/acsnano.4c09156
ACS Nano 2024, 18, 28910−28923

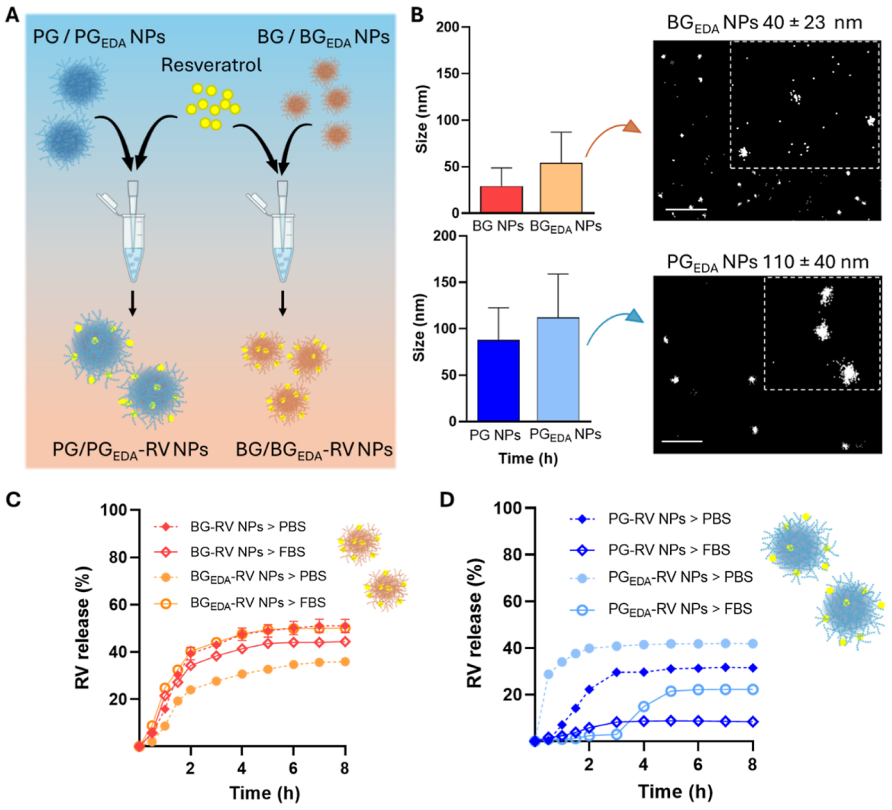

Figure 1. Glycogen NP stability, integrity, and drug release in the presence of serum. (A) Schematic representation of loading of unmodified and EDA-modified glycogen NPs with RV. (B) Stability of NPs after incubation in 10% FBS for 3 h, as measured by DLS and STORM imaging. Scale bars: 1 μm. Release kinetics of RV from (C) BG NPs and BG$_{EDA}$ NPs and (D) PG NPs and PG$_{EDA}$ NPs in phosphate-buffered saline (PBS) and 10% FBS.

enable glucose-responsive insulin release in two distinct diabetic mouse models, with optimal bioavailability, pharmacokinetics, and safety profiles.[27] The interaction of native or chemically modified glycogen NPs with numerous cell lines, including cancer cells (prostate, breast, and liver cells) and human umbilical vein endothelial cells, healthy fibroblasts, and monocytes derived from human blood have been widely investigated.[18,23,27−30] Glycogen NPs are known to be internalized by these cells through endocytic processes. Despite these studies, the interplay between internalization efficiency, intracellular trafficking, endosomal escape, degradation, and cargo release with the physicochemical properties of the NPs, such as size, surface charge, morphology, and chemical functionalities, remains elusive. Furthermore, the intracellular fate of glycogen NPs with T cells is yet to be investigated.

In the present study, we examined the interaction of a range of glycogen NPs differing in size, surface charge, and chemical modification with human Jurkat T cells and primary T cells. These cells were specifically selected because immune T cells are notoriously challenging cells to transfect.[31] The key barriers to transfecting primary T cells and Jurkat T cells are the nonphagocytic nature of these cells, the low level of negatively charged heparin sulfate proteoglycans on the cell membrane that limits the internalization of cationic NPs, and the slow endosomal acidification process that inhibits endosomal escape of NPs through the proton sponge effect.[31] To enable the internalization of NPs in T cells, receptor-targeting antibodies (anti-CD3, CD4 CD7, and CD8) are chemically conjugated to NPs.[32] However, the conjugation of antibodies to NPs is often laborious, resulting in complex and costly manufacturing processes. In addition, antibody−NP conjugates may present challenges with stability issues and variable biological activity.[32]

Hence, there is a need for the development of NP platforms for the effective delivery of therapeutics to T cells. To monitor the internalization and functionality of glycogen NPs in T cells, we used J-Lat A2 cells, a cell line derived from human Jurkat cells infected with a single copy of HIV-1 provirus engineered to express green fluorescent protein (GFP) upon activation.[33−35] We engineered several nanosugar−polyphenol constructs by loading glycogen NPs of different sizes (20 and 80 nm) and surface charge properties (neutral and positively charged) with RV, a natural polyphenol found in grapes, berries, and peanuts.[36] RV has been shown to reactivate latent HIV-1 by stimulating histone acetylation and heat shock protein expression in J-Lat A2 cells.[37] Despite RV having been screened as a latency-reversing agent, the naked drug has shown low bioavailability and is rapidly metabolized in the body.[37] To address this limitation, developing a biodegradable and nonimmunogenic nanocarrier for RV is desirable. The interactions and bioactivities of the different glycogen NPs on J-Lat A2 cells—in terms of cellular uptake kinetics, intracellular trafficking, and reactivation of latent HIV-1—were evaluated and compared using confocal microscopy and flow cytometry.

We found that all glycogen NPs engaged with J-Lat A2 cells regardless of the charge and size of the NPs. PG$_{EDA}$ NPs strongly bound to the cell membrane and were internalized by J-Lat A2 cells. However, they remained confined in the endocytic vehicles, with moderate expression of GFP. In contrast, BG$_{EDA}$ NPs that were efficiently internalized by cells

https://doi.org/10.1021/acsnano.4c09156
ACS Nano 2024, 18, 28910−28923

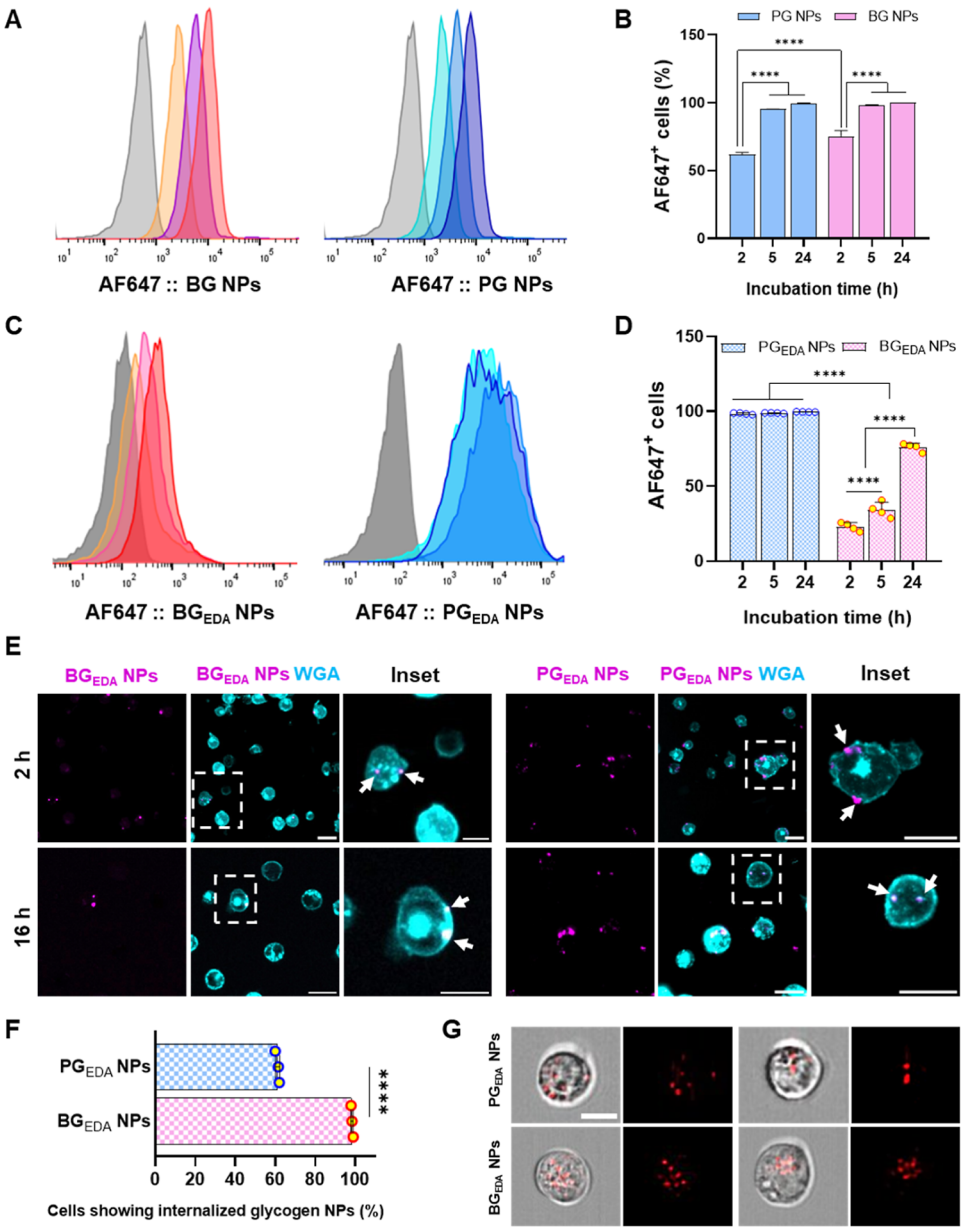

Figure 2. Glycogen NPs engage with immune T cells. (A) Histogram representation and (B) AF647-positive J-Lat A2 cell quantification after incubation with BG NPs or PG NPs labeled with AF647 dye. (C) Histogram representation and (D) AF647-positive J-Lat A2 cell quantification after incubation with BG_{EDA} NPs or PG_{EDA} NPs labeled with AF647 dye. Statistical analyses were performed using two-way analysis of variance (ANOVA), followed by Tukey's multiple comparisons test, $n \geq 3$; *$p < 0.05$, **$p < 0.01$, ***$p < 0.001$, ****$p < 0.0001$. (E) Representative confocal images of J-Lat A2 cells [wheat germ agglutinin (WGA), cyan] after exposure to AF647-labeled PG_{EDA} NPs (pink) or AF647-labeled BG_{EDA} NPs (pink) for 2 and 16 h; scale bars: 20 μm. (F) Quantification of cells with internalized glycogen NPs and (G) representative images from imaging flow cytometry analysis of J-Lat A2 cells exposed to AF647-labeled PG_{EDA} NPs or AF647-labeled BG_{EDA} NPs for 24 h. Statistical analysis performed by unpaired *t*-test ($n = 3$, ****$p < 0.0001$). Scale bar: 10 μm.

generated higher T cell reactivation of proviral GFP expression owing to their higher endosomal escape efficiency. Furthermore, BG_{EDA} NPs engaged with primary blood human T cells (>90% NPs association) and enabled the delivery of mRNA.

Overall, the current study demonstrates the capability of antibody-free glycogen NPs to engage with immune T cells, allowing the intracellular delivery of small drug molecules or mRNA. These findings provide an avenue for the rational design of glycogen NPs through modulation of their size, surface charge, and functional groups to control the cellular uptake, intracellular trafficking, and release of different therapeutic cargos in T cells.

RESULTS AND DISCUSSION

Preparation and Characterization of Glycogen NPs Loaded with RV. Dendrimer-like glycogen NPs derived from sweet corn and bovine liver, hereafter referred to PG NPs and BG NPs respectively, were used in this study. PG NPs displayed a hydrodynamic diameter of 83 ± 24 nm and a ζ-potential value of −1 ± 2 mV, whereas BG NPs exhibited a hydrodynamic diameter of 24 ± 8 nm and ζ-potential of −6 ± 2 mV, as determined by dynamic light scattering (DLS) and electrophoretic mobility measurements (Table S1).

Ethylenediamine (EDA) groups were incorporated into PG NPs and BG NPs through a reductive amination reaction to

https://doi.org/10.1021/acsnano.4c09156
ACS Nano 2024, 18, 28910−28923

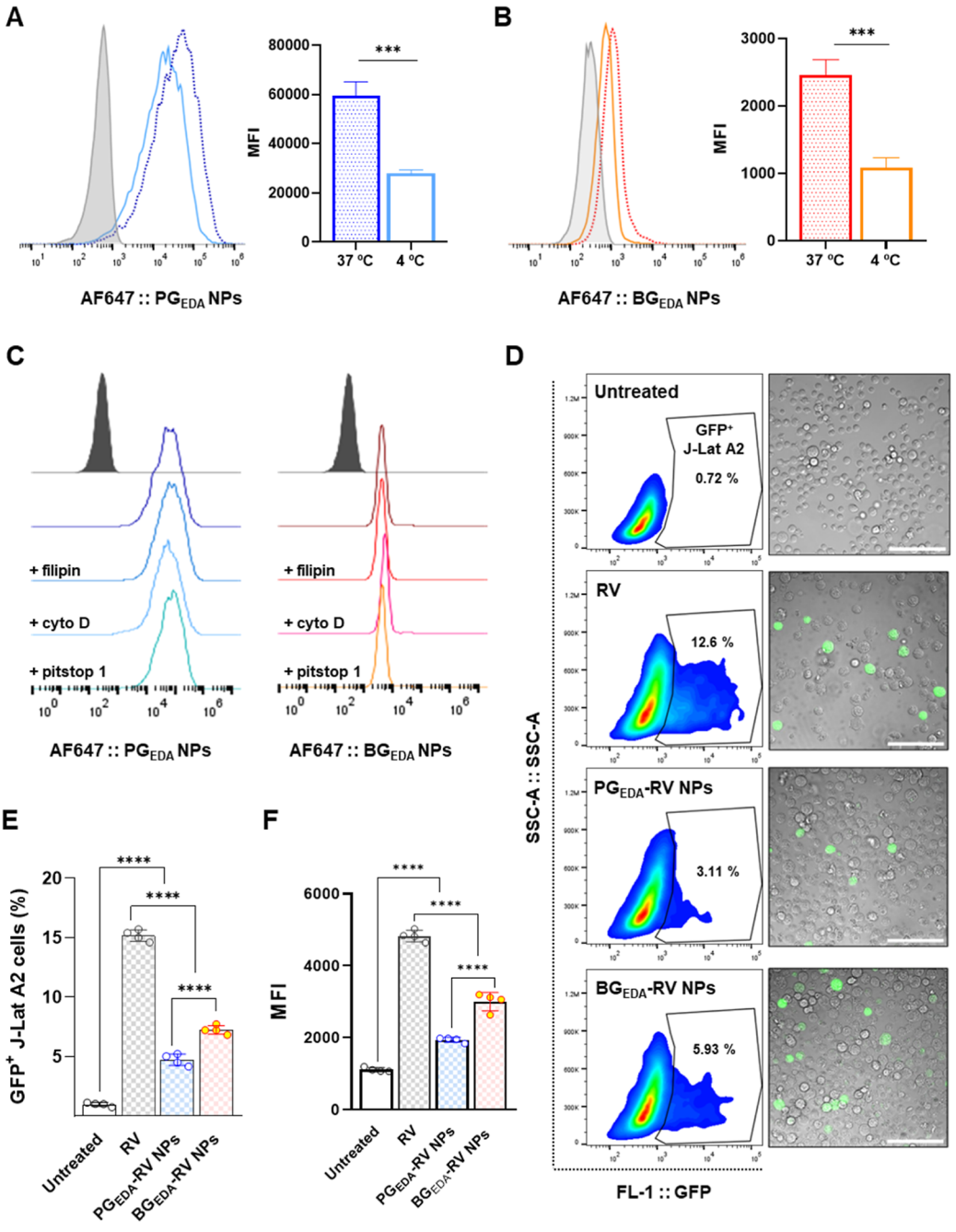

Figure 3. RV-loaded glycogen NPs can reactivate latent HIV in J-Lat A2 cells. Association of (A) PG$_{EDA}$ NPs or (B) BG$_{EDA}$ NPs with J-Lat A2 cells and MFI estimation after 2 h incubation at 4 and 37 °C. (C) Effect of endocytic inhibitors (filipin, cytochalasin D (cyto D), and pitstop 1 inhibiting macropinocytosis, caveolae- and clathrin-dependent endocytosis, respectively) on the association of PG$_{EDA}$ NPs or BG$_{EDA}$ NPs with J-Lat A2 cells. (D) Flow cytometry representative dot plots for the expression of GFP in J-Lat A2 cells exposed to free drug and drug-loaded glycogen NPs at a final concentration of 40 μM for 48 h. Representative confocal images of activated J-Lat A2 cells expressing GFP; scale bars: 100 μm. (E) GFP expression and (F) MFI quantification in J-Lat A2 cells based on flow cytometry results. Statistical analyses were performed by one-way ANOVA, followed by Tukey's multiple comparisons test, $n = 4$; *$p < 0.05$, **$p < 0.01$, ***$p < 0.001$, ****$p < 0.0001$.

obtain PG$_{EDA}$ NPs and BG$_{EDA}$ NPs, respectively.[23,29] The degree of substitution (DS) with EDA for both NPs was 6%, as determined by ^{1}H NMR spectroscopy (Figure S1 and Table S2). The ζ-potentials and hydrodynamic diameters of PG$_{EDA}$ NPs and BG$_{EDA}$ NPs are listed in Table S1. PG$_{EDA}$ NPs and BG$_{EDA}$ NPs displayed positive ζ-potential values of 23 ± 5 and 10 ± 6 mV, respectively, indicating that the amination of the polysaccharide chains conferred a positively charged surface to both NPs (Table S1). However, PG$_{EDA}$ NPs exhibited a higher charge density. PG$_{EDA}$ NPs and BG$_{EDA}$ NPs (following surface modification) displayed comparable particle sizes to the nonmodified NPs (Table S1). To assess the structural stability of the NPs in both extracellular and intracellular environments, their biodegradability was evaluated by the α-amylase and β-amylase digestion assays. The analysis was performed at 37 °C for 3 h using amylase levels typically found in blood and the lysosomal compartments. The data shown in Table S1 indicated that both PG NPs and PG$_{EDA}$ NPs were resistant

https://doi.org/10.1021/acsnano.4c09156
ACS Nano 2024, 18, 28910−28923

to α-amylase digestion, undergoing only 7% degradation, whereas BG NPs and BG_{EDA} NPs degraded partially, up to 25% and 15% respectively. After treatment with β-amylase for 3 h, ~40% of degradation was determined for both unmodified PG NPs and BG NPs. In contrast, PG_{EDA} NPs and BG_{EDA} NPs were resistant to β-amylase digestion, with only 12% and 9% of degradation observed, respectively.

The colloidal stability and integrity of the NPs were further investigated by incubating the NPs in 10% fetal bovine serum (FBS) solution (containing α-amylase) for 3 h. All NPs remained well dispersed over the incubation period examined. Only a slight increase in size was noted for BG NPs (29 ± 20 nm) and PG NPs (88 ± 34 nm), whereas BG_{EDA} NPs and PG_{EDA} NPs displayed an increase in size and polydispersity, as indicated by DLS analysis (54 ± 32 and 112 ± 46 nm, respectively) and, at the nanoscale, by stochastic optical reconstruction microscopy (STORM) imaging and clustering analysis of localizations (Figures 1B and S2). These results highlight that slightly negative BG NPs and PG NPs have limited interactions with serum protein owing to the high surface hydration, whereas the cationic PG_{EDA} NPs and BG_{EDA} NPs likely interact with the negatively charged serum albumin by electrostatic interactions. Overall, these results suggest that all the investigated NPs maintain their structural integrity in extracellular environments (i.e., cell culture medium) with limited effect on their size and dispersibility. Furthermore, chemical modification with EDA (even at a low DS of 6%) prevents rapid degradation by hydrolytic enzymes present in the intracellular milieu.

Next, RV was loaded into the unmodified and EDA-modified NPs by mixing the polyphenol with the NPs in aqueous solution and purifying the loaded NPs by spin column to obtain BG-RV NPs, BG_{EDA}-RV NPs, PG-RV NPs, and PG_{EDA}-RV NPs (Figure 1A). RV molecules (polyphenol) can diffuse into the porous NPs and interact with the highly branched polysaccharide backbone by hydrogen bonding.[20] Intermolecular dimerization of RV molecules by $\pi-\pi$ stacking interactions within the dendrimer-like structure of glycogen is also possible. The RV loading of the neutral and aminated NPs, estimated as weight ratio, was comparable (Table S1), suggesting that functionalization with EDA does not influence drug loading. Drug release kinetics were studied in PBS and 10% FBS to mimic in vitro cellular experimental conditions. Figure 1C illustrates that approximately 25−40% of RV was released from BG-RV NPs and BG_{EDA}-RV NPs in the first 2 h of incubation in both PBS and 10% FBS. A stark difference in the RV release kinetics was observed for PG-RV NPs and PG_{EDA}-RV NPs in the presence of serum proteins. Approximately 30−40% of RV was released from PG-RV NPs and PG_{EDA}-RV NPs in PBS in the first 2 h of incubation, whereas only 5 and 2% of RV was released from PG-RV NPs and PG_{EDA}-RV NPs, respectively, within 2 h of incubation in FBS (Figure 1D). These findings suggest that both unmodified and EDA-modified glycogen NPs provide a platform for the sustained release of RV in cell culture media. In particular, the interactions with serum proteins provide an effective barrier to RV diffusion and enable a slow release of the drug from PG NPs and PG_{EDA} NPs.

Glycogen NPs Engage with Human Immune T Cells. Subsequently, we verified that all unmodified and EDA-modified glycogen NPs (Figure S3) were not toxic upon interaction with immune T cells using the J-Lat A2 cell line. It is known that immune T cells grow in suspension, which poses a challenge for NP internalization.[38] PG NPs and BG NPs equally labeled with Alexa Fluor 647 (AF647) were incubated with J-Lat A2 cells for 2, 5, and 24 h. The flow cytometry studies revealed that both PG NPs and BG NPs bound to J-Lat A2 cells, and the degree of association increased with longer exposure times (Figure 2A,B). The quantification of cells positive for AF647 and mean fluorescence intensity (MFI) indicated a faster cellular association kinetics with a higher association efficiency for BG NPs than for PG NPs (Figures 2B and S4A,B).

Similar studies were performed using AF647-labeled PG_{EDA} NPs and BG_{EDA} NPs. The results in Figure 2C,D revealed a significant difference in the association kinetics and internalization efficiency of the cationic PG_{EDA} NPs and BG_{EDA} NPs with J-Lat A2 T cells. PG_{EDA} NPs displayed a rapid and substantial association with T cells with 100% positive cells observed after 2 h of incubation, whereas BG_{EDA} NPs were slowly internalized at a lower efficiency, showing 23 ± 3%, 34 ± 5% and 76 ± 3% association after 2, 5, and 24 h of incubation, respectively (Figures 2C,D and S4C,D). Confocal microscopy imaging of the cells treated with PG_{EDA} NPs or BG_{EDA} NPs with DS = 6, confirmed a higher number of PG_{EDA} NPs than BG_{EDA} NPs associated with J-Lat A2 after 2 and 16 h of incubation (Figure 2E). Using imaging flow cytometry, we could discriminate between NPs bound to the cell membrane and those that had been internalized. The results in Figures 2F,G and S5 show that the BG_{EDA} NPs that are bound to the membrane are internalized by J-Lat A2 cells at a higher rate with nearly 100% cells positive for NP internalization when compared with PG_{EDA} NPs, where approximately 60% of the total number of cells positive for AF647 had internalized the NPs.

To further corroborate these findings, we studied the affinity of the NPs for the cell membrane by exposing J-Lat A2 cells to BG_{EDA} NPs or PG_{EDA} NPs at 4 °C, when energy-dependent endocytosis of NPs is suppressed. Figure 3A,B indicated that PG_{EDA} NPs displayed approximately 20-fold higher affinity for cell membrane than BG_{EDA} NPs. The comparison of the cell association at 4 and 37 °C revealed a reduction in the cell association of both BG_{EDA} NPs and PG_{EDA} NPs (approximately 2-fold MFI reduction) at the lower temperature, indicating that both NPs are internalized via energy-dependent endocytic processes (Figures 3A,B and S6).

The interplay of size and surface charge on cell association was assessed by examining NP−cell association using (1) PG_{EDA} and BG_{EDA} NPs with a comparable ζ-potential value and (2) BG_{EDA} NPs with varying surface charges. To examine the effect of NP size, the surface charge of PG_{EDA} and BG_{EDA} NPs was controlled by increasing the degree of amine functionalization within 6−20%. The flow cytometry results showed that BG_{EDA} NPs (ζ-potential of 20 mV) associated rapidly with J-Lat A2 cells within 2 h of incubation (Figure S7A,B), similar to what was observed for PG_{EDA} NPs (ζ-potential of 23 mV) in Figure 2C,D. However, flow imaging analysis confirmed that BG_{EDA} NPs (ζ-potential, 20 mV) were internalized by J-Lat A2 cells at a higher degree of ~75% than PG_{EDA} NPs (ζ-potential, 23 mV) (~60%) within the 24 h incubation period examined (Figure S7C). The cellular association of the NPs with a higher ζ-potential value (i.e., ~50 mV) was also studied. Similar to the results discussed above, PG_{EDA} NPs displayed a higher cell association than BG_{EDA} NPs (Figure S7D,E). Although both types of glycogen NPs resulted in 100% cell association after 5 h of incubation,

https://doi.org/10.1021/acsnano.4c09156
ACS Nano 2024, 18, 28910−28923

PG_{EDA} NPs displayed approximately 20-fold higher MFI values. To examine the effect of ζ-potential, the association of BG_{EDA} NPs with different ζ-potential values (i.e., 10, 20, and 50 mV) was investigated. As expected, a higher NP surface charge resulted in a higher cell association (Figure S7F,G). The same trend was observed for the PG_{EDA} NPs, displaying a positive correlation between surface charge and the level of cellular association (Figures S7D,E and 2C,D).

Overall, these data support our initial hypothesis that smaller glycogen NPs (BG_{EDA} NPs) are internalized by immune T cells more efficiently than larger NPs (PG_{EDA} NPs). However, despite the slow and less efficient association displayed by BG_{EDA} NPs (10 mV), these NPs showed a higher degree of internalization within the 24 h incubation period examined (Figure 2F) than BG_{EDA} NPs (20 mV) or PG_{EDA} NPs (20 mV) (Figure S7C). This indicates that the strong affinity of NPs to the cell membrane does not necessarily positively correlate with the internalization efficiency of NPs. As the higher positive charge also accounts for higher toxicity, glycogen NPs with the lowest degree of EDA functionalization (DS = 6) were selected as the optimal system for further experiments.

To obtain insight into the mechanism underlying the internalization of glycogen NPs, a set of experiments using endocytosis inhibitors was performed. Cytochalasin D, filipin from *Streptomyces filipinensis*, and pitstop 1 were used to block macropinocytosis, caveolae- and clathrin-dependent endocytosis, respectively. The results in Figure 3C show that these inhibitors do not cause a significant effect on glycogen NP association with J-Lat A2 cells, suggesting that alternative mechanisms are responsible for the interaction of glycogen with T cells. We hypothesize that the positively charged glycogen NPs can engage with the heparan sulfate proteoglycan present on the cell membrane of T cells via electrostatic interactions and hydrogen bonding. Although T cells have a low level of heparan sulfate on the membrane, the dendrimer-like structure of PG_{EDA} NPs and BG_{EDA} NPs may be pivotal in controlling their multivalent binding to heparan sulfate domains that upon clustering facilitates the internalization process.[39] Though the exact mechanisms underlining heparan sulfate clustering are yet to be elucidated, it is known that charge neutralization between cationic NPs and the anionic heparan sulfate proteoglycan leads to the formation of neutral complexes that are internalized.[39] Another hypothesis is that the NP-mediated cross-linking of heparan sulfate may induce actin rearrangement, leading to the endocytosis of NPs.[39] The large PG_{EDA} NPs can likely engage more efficiently with the cell membrane of T cells because they can exploit more binding sites unlike the small low charge density BG_{EDA} NPs. In addition, the adhesiveness of BG_{EDA} NPs to the cell membrane may be diminished by electrostatic interactions with albumin.[40] To understand the role of the polysaccharide backbone in the association of NPs with J-Lat A2 cells, EDA-functionalized dextran NPs ($Dextran_{EDA}$ NPs), with comparable surface charge (8 mV) and size (18 ± 6 nm) to those of BG_{EDA} NPs, were incubated with J-Lat A2 cells. The flow cytometry results in Figure S8A−C showed that $Dextran_{EDA}$ NPs labeled with AF647 gradually associated with J-Lat A2 cells over 24 h of incubation. The association of the $Dextran_{EDA}$ NPs was also assessed after 2 h of incubation at 4 and 37 °C. At the lower temperature, when energy-dependent endocytosis is limited, a significantly lower degree of association of $Dextran_{EDA}$ NPs with J-Lat A2 cells was observed than at the higher temperature. Additionally, flow imaging analysis showed that the $Dextran_{EDA}$ NPs were nearly 100% internalized after 24 h (Figure S8D), as previously observed for BG_{EDA} NPs. These results indicate that the multivalent cationic polysaccharide backbone of either glycogen or dextran NPs is likely enabling association of the NPs with immune T cells.

RV-Loaded Glycogen NPs Can Reactivate Latent HIV in J-Lat A2 Cells. Based on the lower degradability profiles exhibited by the positively charged NPs in the extracellular environment and their contrasting cell association profiles, we performed a comparative analysis of the nano−bio interactions of PG_{EDA} NPs and BG_{EDA} NPs with J-Lat A2 immune T cells. Specifically, the NP-mediated reactivation of latent HIV-1 by RV delivery and intracellular trafficking were investigated.

To evaluate the bioactivity of glycogen NPs in immune cells, J-Lat A2 cells were treated with glycogen NPs preloaded with RV (Figure 1A). The effects of drug dosage and incubation time (10−80 μM, 48 h) that would elicit GFP expression without a significant impact on cell viability were first assessed. Negligible cell death (<20%) and a detectable value of GFP expression of 22 ± 3% (Figure S9A,B) were obtained at an optimal RV dosage of 40 μM, which was used in subsequent experiments. Next, J-Lat A2 cells were exposed to the free drug (RV) or glycogen NPs containing RV (BG-RV NPs, BG_{EDA}-RV NPs, PG-RV NPs, PG_{EDA}-RV NPs) at a final concentration of 40 μM for 48 h. The results of GFP expression, as determined by flow cytometry, indicated an increase in the number of GFP-expressing T cells (≥5%) for all samples treated in the presence of RV (Figure S10).

As expected, the free drug readily permeated into the cells by passive diffusion and triggered HIV-1 reactivation in 15 ± 1% cells after 48 h incubation (Figures 3D and S10). This finding agrees with previously published data, which reveal that RV acts as a natural latency reversing agent and enhances HIV gene expression in a dose-dependent manner.[41] When mediated by RV-loaded glycogen NPs, approximately 5−9% of cells underwent provirus reactivation (Figures 3D and S10B). It is worth noting that the lower stimulatory activity of all tested NPs compared to the free drug (5−9% vs 15% reactivation) strongly suggests that the payload drug is released inside the cells upon internalization and does not leach out to the extracellular environment. The apparent lower reactivation degree observed for all glycogen NPs, which are internalized via endocytic active processes, might be attributed to the segregation of the glycogen NPs in the endolysosomal compartments that limit rapid access of RV to the cytosolic target. It is reported that RV acts by triggering the phosphorylation of heat shock factor (HSF1) in the cytosol, resulting in the translocation of HSF1 into the nucleus to induce the transcription of many genes including the HIV gene in J-LAT A2 cells.[42]

Interestingly, BG_{EDA}-RV NPs resulted in approximately 1.5-fold higher activation of J-Lat A2 cells (7.3 ± 0.4%) than PG_{EDA}-RV NP (4.7 ± 0.5%), with corresponding 1.5-fold higher GFP MFI values (3004 ± 255 vs 1940 ± 68) (Figure 3E,F). Therefore, we speculate that the intracellular trafficking and endosomal escape of BG_{EDA}-RV NPs and PG_{EDA}-RV NPs are also important for reactivation of immune T cells by RV.

To gain insights into the mechanism of the intracellular trafficking of BG_{EDA} NPs and PG_{EDA} NPs and support our hypothesis, NP colocalization studies were conducted by immunostaining the organelles involved in the endolysosomal pathway. After incubation of J-Lat A2 cells for 5 h with AF647-

https://doi.org/10.1021/acsnano.4c09156
ACS Nano 2024, 18, 28910−28923

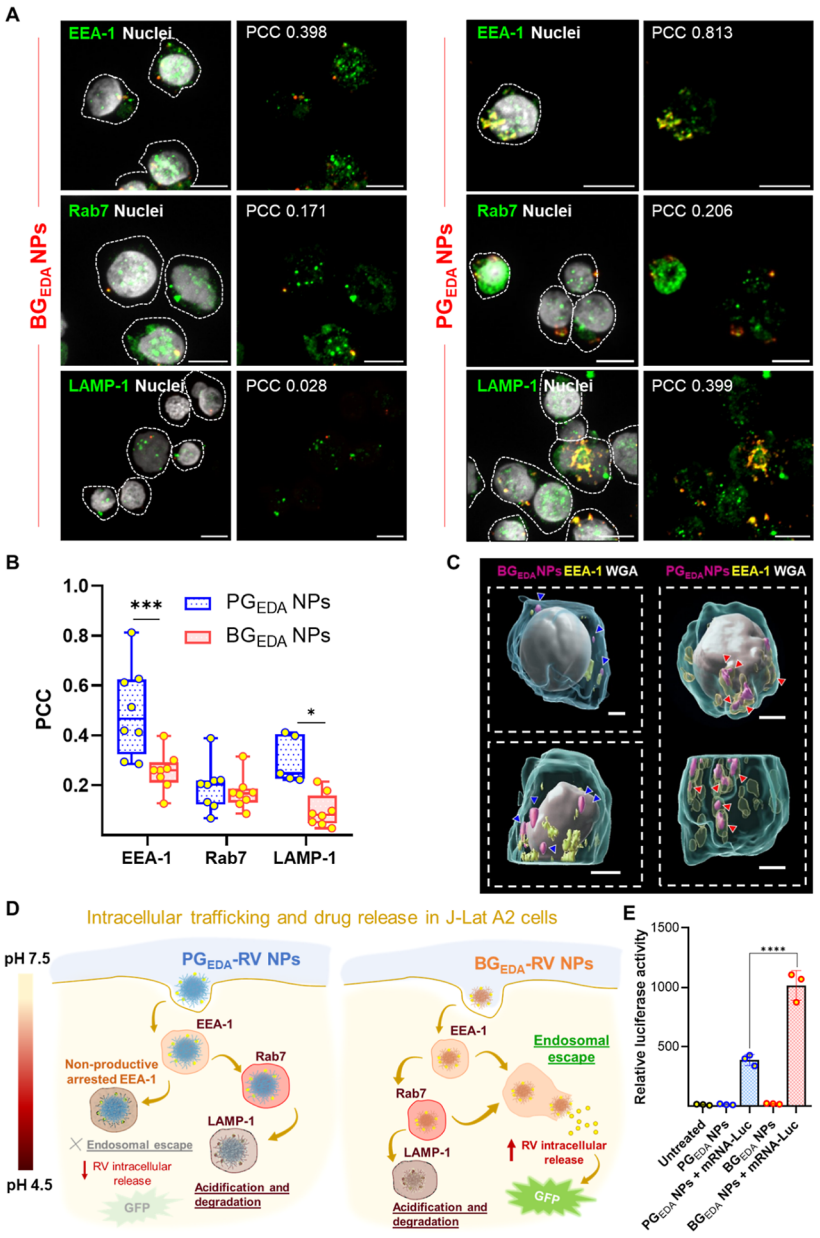

Figure 4. Endosomal escape of PG$_{EDA}$ NPs and BG$_{EDA}$NPs in immune T cells. (A) Representative confocal images of J-Lat A2 cells treated with AF647-labeled PG$_{EDA}$ NPs or BG$_{EDA}$ NPs (red) for 5 h and further incubated for 19 h. Cells were stained with antibodies against EEA-1 for early endosomes, Rab7 for late endosomes, and LAMP-1 for lysosomes. Scale bars: 20 μm. (B) Colocalization of glycogen NPs with early (EEA-1) and late (Rab7) endosomes, and lysosomes (LAMP-1) after 24 h incubation, as assessed by PCC. Statistical analysis was performed by two-way ANOVA, followed by Tukey's multiple comparisons test; *$p < 0.05$, **$p < 0.01$, ***$p < 0.001$, ****$p < 0.0001$. (C) IMARIS 3D reconstruction of J-Lat A2 cells after incubation with PG$_{EDA}$ NPs or BG$_{EDA}$ NPs (magenta) for 24 h and stained for early endosomes (EEA1, yellow), WGA for cell membrane (cyan), and Hoechst 33342 for nuclei (white). Blue arrows indicate BG$_{EDA}$ NPs escaping from early endosomes. Red arrows indicate PG$_{EDA}$ NPS entrapped within the EEA1 vesicles. Scale bars: 3 μm. (D) Schematic representation of the proposed mechanism of intracellular trafficking of PG$_{EDA}$ NPs and BG$_{EDA}$ NPs within J-Lat A2 cells. (E) Relative luciferase activity measured by luminescence after transfection of J-Lat A2 cells with glycogen NPs + mRNA-Luc (1 μg mRNA-Luc). Statistical analysis was performed by one-way ANOVA followed by followed by Tukey's multiple comparisons test ($n = 3$; ****$p < 0.0001$).

labeled BG$_{EDA}$ NPs or PG$_{EDA}$ NPs (red), the cells were washed to remove the noninternalized NPs and further incubated for 19 h. Next, the J-Lat A2 cells were fixed and stained for early endosomes (early endosome antigen 1, EEA-1), late endosomes (Rab7), and lysosomes (lysosomal-associated membrane protein 1, LAMP-1) (Figures 4A and S11, green). The cells were then analyzed by confocal microscopy followed by image analysis using ImageJ to determine the Pearson's correlation coefficient (PCC, Figure 4B). PCC serves as an indicator for NP colocalization with the different endolysosomal compartments. Of note, NP clusters were imaged inside cells (Figure 4A), indicating that the NPs undergo clustering on the cell membrane upon internalization or during endocytic organelle fusion processes. BG$_{EDA}$ NPs displayed low PCC values for all endocytic vesicles, 0.26 ± 0.08 (EEA-1), 0.17 ± 0.07 (Rab7), and 0.10 ± 0.07 (LAMP-1), indicating efficient endosomal escape (Figure 4B). These findings are in agreement with our previously reported work. It was

https://doi.org/10.1021/acsnano.4c09156
ACS Nano 2024, 18, 28910−28923

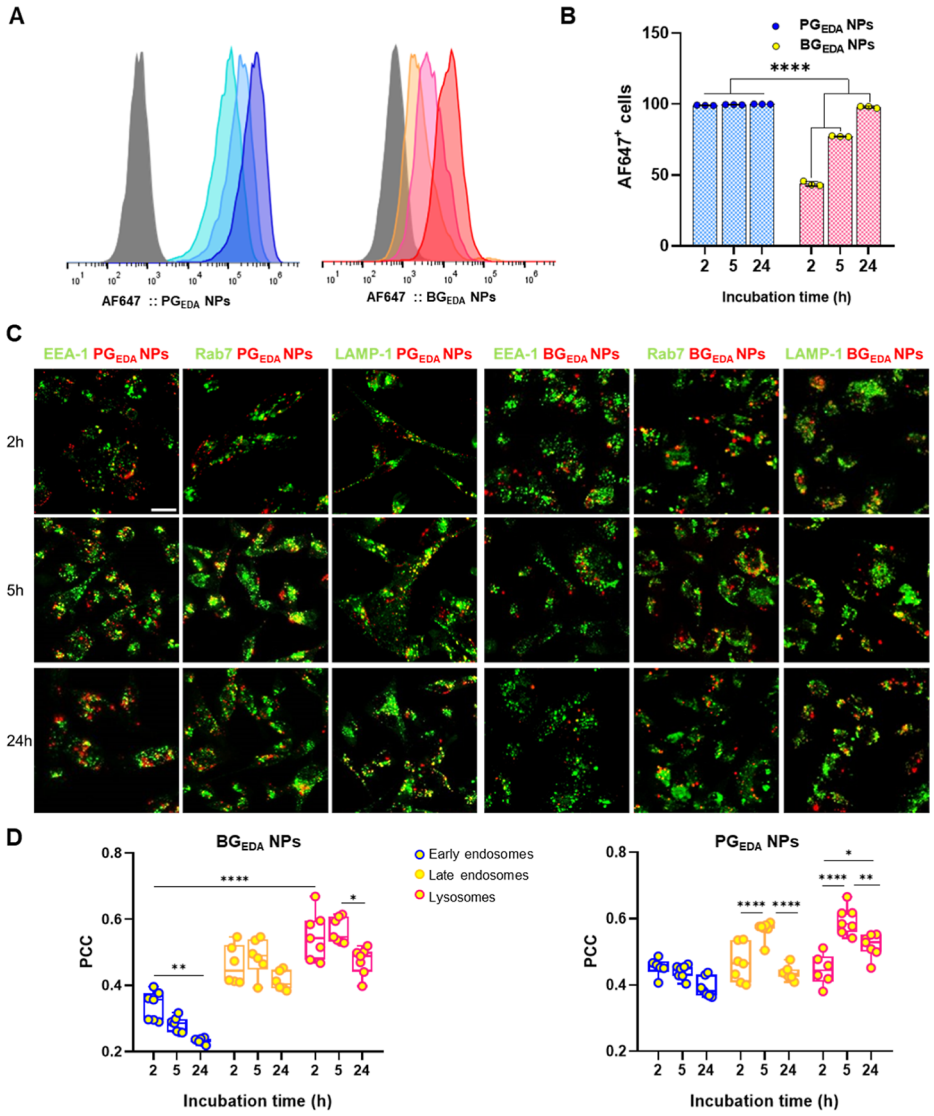

Figure 5. BG_{EDA} NPs and PG_{EDA}NPs intracellular trafficking in MDA-MB-231 breast cancer cells. (A) Histogram representation of cells after incubation with glycogen NPs labeled with AF647 dye. (B) AF647-positive cell quantification based on flow cytometry analysis. Statistical analysis was performed by two-way ANOVA, followed by Tukey's multiple comparison test, $n = 4$. (C) Representative confocal images of MDA-MB-231 cells stained in green for early endosomes (EEA-1), late endosomes (Rab7), and lysosomes (LAMP-1) after incubation with AF647-labeled nanosugars (red) for 2, 5, and 24 h. Scale bar in all images: 100 μm. (D) Colocalization of glycogen NPs with early and late endosomes, and lysosomes as a function of incubation time, as assessed by PCC analysis. Statistical analyses were performed by two-way ANOVA, followed by Tukey's multiple comparison test; *$p < 0.05$, **$p < 0.01$, ***$p < 0.001$, ****$p < 0.0001$.

demonstrated through super-resolution microscopy that in cancer cells, the endosomal escape of BG_{EDA} NPs is triggered by the proton sponge effect mechanism, as the secondary amines in EDA exhibit buffering properties and possess pK_a (6.5) within the range of endosomal pH.[29] Specifically, we demonstrated, by direct imaging of individual BG_{EDA} NPs and early endosomes with nanoscale resolution, that the endocytosed branched cationic BG_{EDA} NPs caused an osmotic imbalance, resulting in endosome swelling and rupture.[29]

In contrast, PG_{EDA} NPs appeared mainly colocalized with early endosomes (EEA-1, PCC = 0.50 ± 0.18) and the lysosomes (LAMP-1, PCC = 0.30 ± 0.10) (Figure 4A,B). The confinement of PG_{EDA} NPs in the early endosomes is visible by 3D reconstruction of the cells performed with IMARIS (Figure 4C, red arrows). Conversely, BG_{EDA} NPs were detected mostly in the cytosol (Figure 4C, blue arrows). It has been recently reported that the escape of macromolecules and lipid cationic NPs is restricted to the early endosomal compartments before conversion into late endosomes or recycling endosomes, whereas late endosomes and lysosomes are unlikely to promote endosomal escape.[43] Furthermore, prolonged and substantial retention of NPs in the endosomes has been reported to impair endosomal acidification and cause NPs to accumulate in defective compartments unproductive for delivery.[43] The finding that PG_{EDA} NPs primarily accumulate in the early endosomes with limited transition to late endosomes indicates that trafficking of NPs is arrested in J-LAT A2 cells and the escape from the arrested endosomes is typically negligible (Figure 4D).

In addition, unlike other cell types, immune T cells typically exhibit a slow endosomal acidification process up to 4 h, which may further inhibit the endosomal escape of NPs through the proton sponge effect.[29] Taken together, our data suggest that the engulfment of early endosomes may slow the release of RV

https://doi.org/10.1021/acsnano.4c09156
ACS Nano 2024, 18, 28910−28923

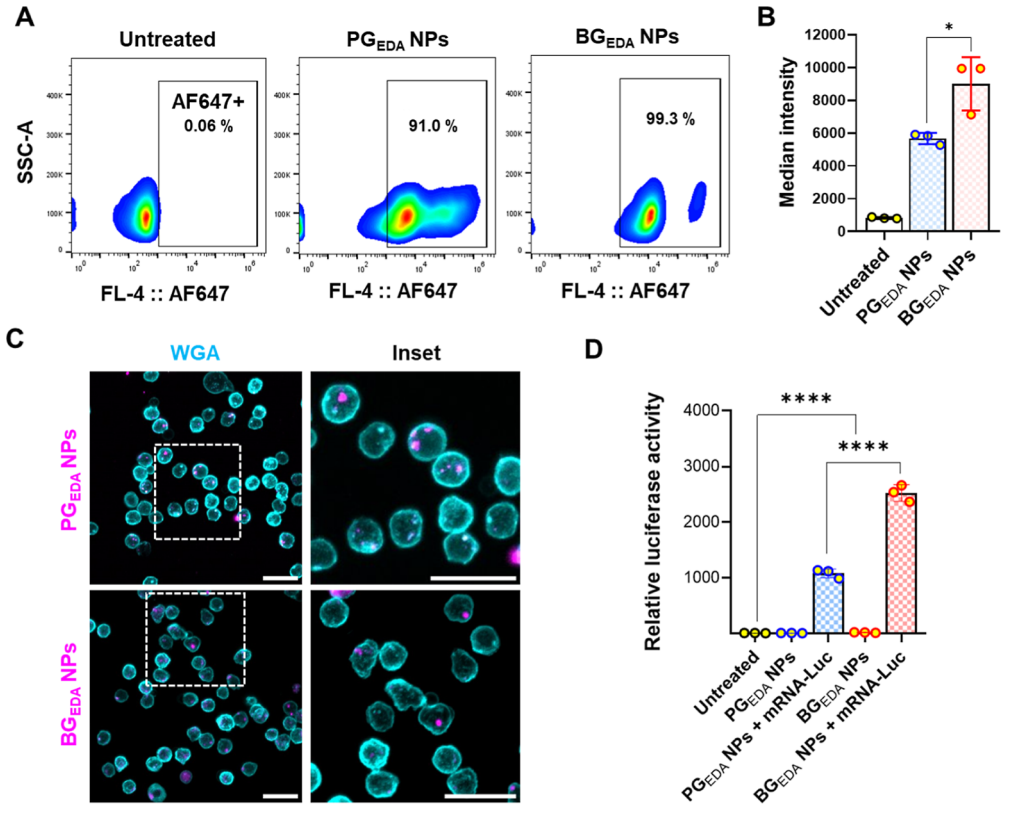

Figure 6. Glycogen NPs can transfect primary human T cells. Association of (A) PG_{EDA} NPs and BG_{EDA} NPs with primary T cells and (B) median intensity estimation after 24 h incubation. (C) Representative confocal images of primary T cells after incubation for 24 h with cationic glycogen NPs; scale bars: 20 μm. (D) Relative luciferase activity measured by luminescence after transfection of human primary T cells with glycogen NPs + mRNA-Luc (1 μg mRNA-Luc). Statistical analysis was performed by one-way ANOVA, followed by Tukey's multiple comparisons test, $n = 3$; *$p < 0.05$, **$p < 0.01$, ***$p < 0.001$, ****$p < 0.0001$.

from PG_{EDA} NPs, resulting in a lower GFP expression (Figure 4D). In contrast, BG_{EDA} NPs are amenable to endosomal escape and the effective deployment of RV in the cytosol enhances the expression of GFP (Figure 4D).

Association and Endosomal Escape of BG_{EDA} NPs and PG_{EDA} NPs in Human Breast Cancer Cells. As a comparative study, we investigated the association and intracellular behavior of BG_{EDA} NPs and PG_{EDA} NPs in breast cancer cells (MDA-MB-231), which typically have a negatively charged cell membrane and, unlike T cells, display a rapid endosomal acidification process. The findings in Figure 5A,B indicate that PG_{EDA} NPs rapidly and efficiently associated with MDA-MB-231 cells and reached a plateau after 2 h of incubation, whereas BG_{EDA} NPs exhibited a gradual and approximately an order of magnitude less pronounced association over the 24 h incubation period examined. This is consistent with the study conducted on J-Lat A2 cells (Figure 2D). To track the intracellular transport of NPs upon endocytosis, we performed a colocalization study after 2, 5, and 24 h of incubation with the NPs (red), with a washing step at 2 h to introduce fresh medium and remove excess NPs in suspension. Cancer cells were fixed and stained for early endosomes (EEA-1), late endosomes (Rab7), and lysosomes (LAMP-1) (Figure 5C, green). The BG_{EDA} NPs showed limited colocalization with early endosomes after incubation for 2 h (PCC 0.34 ± 0.04), which further declined over time (PCC 0.23 ± 0.01 at 24 h) (Figure 5D). This progressive reduction in colocalization of BG_{EDA} NPs with early endosomes is indicative of effective endosomal escape and cytosolic release of NPs. However, unlike the observations made in J-LAT A2 cells, in cancer cells, a significant number of BG_{EDA} NPs were transferred to late endosomes and lysosomes (PCC 0.4−0.6), where they are likely degraded. Furthermore, PG_{EDA} NPs were evenly found colocalized with all organelles over the incubation period examined, exhibiting PCC values ranging from 0.4 to 0.6. This suggests that PG_{EDA} NPs can transit from early to late endosomes and lysosomes after internalization. The decrease in colocalization of PG_{EDA} NPs with late endosomes and lysosomes at 24 h incubation can be likely attributed to their degradation, while the slight decrease in PCC values for early endosome colocalization indicates a less efficient endosomal escape, corroborating the findings observed in the J-Lat A2 cell studies.

Glycogen NPs Deliver mRNA to Human Immune T Cells. Next, we investigated the potential of both types of cationic glycogens (PG_{EDA} NPs and BG_{EDA} NPs) to deliver mRNA encoding for luciferase expression (mRNA-Luc) to J-Lat A2 cells. The complexes were characterized by gel electrophoresis to ensure mRNA binding to the glycogen NPs, as shown in Figure S12. It has been shown that the transfection of Jurkat T cells using lipid NPs results in a transient expression of luciferase, with a peak at 24 h that decreases over 96 h.[44] Therefore, for our studies, cells were treated with PG_{EDA} NPs-mRNA-Luc or BG_{EDA} NPs-mRNA-Luc complexes (Figure 4E) or Lipofectamine as a positive control for 24 h (Figure S13). mRNA delivery was detected, resulting in enhanced Luciferase activity in cells treated with both types of carriers (Figure 4E). The transfection results

https://doi.org/10.1021/acsnano.4c09156
ACS Nano 2024, 18, 28910−28923

confirm our previous findings, revealing that BG_{EDA} NPs exhibit >2-fold higher transfection efficiency than PG_{EDA} NPs. This finding supports our observations that BG_{EDA} NPs perform better in transfecting J-Lat A2 cells, likely because of their enhanced endosomal escape.

Finally, we studied the interaction of BG_{EDA} NPs or PG_{EDA} NPs with primary human T cells isolated from buffy coat, which contains lymphocytes, monocytes, and granulocytes. For that purpose, T cells were incubated with NPs for 24 h, following the conditions applied for the studies with J-Lat A2. Flow cytometry analysis confirmed >90% NP association (Figure 6A,B). The effective internalization of BG_{EDA} NPs and PG_{EDA} NPs was also confirmed by confocal microscopy (Figure 6C). Given the potential application of the glycogen NPs in a relevant biological environment, we additionally investigated the association of BG_{EDA} NPs and PG_{EDA} NPs with T cells in the presence of human peripheral blood mononuclear cells (PBMCs) isolated from buffy coat. The PBMCs included B cells, natural killer (NK) cells, monocytes, and dendritic cells (DCs). The association of BG_{EDA} NPs and PG_{EDA} NPs with PBMCs was studied over 2, 5, and 24 h as shown in Figure S14. As expected, significant association of both types of glycogen NPs with phagocytic cells, i.e. monocytes and DCs, was observed as early as 2 h of incubation and continued to increase over the 24 h period of incubation, as shown in Figure S15. The association of both NPs with lymphocytes, i.e. T cells, B cells, and NK cells, could also be detected over time. Notably, T cells exhibited a difference in association with PG_{EDA} NPs and BG_{EDA} NPs, with approximately 50% and 80% positive cells being measured after 24 h, respectively. This confirms the preferential association of the small BG_{EDA} NPs with T cells in complex biological samples.

We next evaluated the ability of the BG_{EDA} NPs and PG_{EDA} NPs to deliver mRNA-Luc. Primary T cells were incubated with PG_{EDA} NPs-mRNA-Luc and BG_{EDA} NPs-mRNA-Luc complexes or Lipofectamine for 24 h (Figure S16). Our results show that the glycogen NPs can successfully deliver mRNA in primary difficult-to-transfect T cells and induce the expression of Luciferase as shown in Figure 6D. In agreement with previous data (Figure 4E), a significantly higher transfection efficiency was observed for BG_{EDA} NPs than for PG_{EDA} NPs (2524 ± 149 vs 1084 ± 80).

Although the lipid-based transfection agent (Figure S16) exhibits 4-fold higher transfection efficiency than BG_{EDA} NPs, lipid-based NPs present several disadvantages, including the requirement of multiple lipid components, low storage stability, toxicity, and immunogenicity. Conversely, BG_{EDA} NPs provide a one-component, natural, antibody-free, non-toxic, and nonimmunogenic[40] platform for the successful delivery of therapeutic molecules in Jurkat T cells and more importantly primary human T cells.

CONCLUSION

The association, intracellular trafficking, and drug delivery properties of antibody-free glycogen NPs, of varying sizes and surface charges, with T cells were evaluated. Flow cytometry and imaging analyses revealed that all NPs were internalized by T cells, including primary T cells isolated from buffy coat peripheral blood. Specifically, small and positively charged glycogen NPs (BG_{EDA} NPs) demonstrated superior endosomal escape, leading to enhanced RV-mediated reactivation of latent HIV-1 in J-Lat A2 T cells. In contrast, larger cationic glycogen NPs (PG_{EDA} NPs) were retained within the early endosomes for prolonged periods, i.e. 24 h, resulting in less efficient delivery of RV into the cytosol. Furthermore, both positively charged glycogen NPs (PG_{EDA} NPs and BG_{EDA} NPs) enabled the successful delivery of mRNA in both difficult-to-transfect cell lines, J-Lat A2, and primary human T cells. BG_{EDA} NPs also showed enhanced transfection efficiency for the delivery of mRNA in primary human T cells. This study highlights the versatility and potential of glycogen NPs in drug delivery to immune T cells by modulating their size and surface charge properties. Furthermore, our study provides insights for the rational design of glycogen NPs for the delivery of nucleic acids, i.e., mRNA, in which endosomal escape is key to realizing effective transfection.

MATERIALS AND METHODS

Materials. Phytoglycogen was purchased from Mirexus Biotechnology Inc. (Guelph, Canada) and bovine liver glycogen was purchased from Sigma-Aldrich. Dialysis tubing (14 kDa) was purchased from Thermo Fisher Scientific. Dulbecco's PBS (DPBS), glycogen from bovine liver, bovine serum albumin (BSA), RV (R5010), α-amylase from *Aspergillus oryzae*, β-amylase from barley, EDA, deuterated water, dimethyl sulfoxide (DMSO), sodium potassium tartrate tetrahydrate, sodium carbonate, sodium bicarbonate, sodium sulfate, copper sulfate pentahydrate, ammonium molybdate, and sodium arsenate dibasic pentahydrate were supplied by Sigma-Aldrich (St. Louis, MO, USA). FBS was purchased from Bovogen Biologicals Pty. Ltd. (Keilor East, Australia). Dulbecco's modified Eagle medium (DMEM), Opti-minimum essential medium (minimum essential medium) (31985070), Roswell Park Memorial Institute (RPMI) 1640 Medium (11875093), trihydrochloride (Hoechst 33342), AlamarBlue cell viability reagent (DAL1100), 4% paraformaldehyde solution (PFA), ethylenediaminetetraacetic acid (EDTA), trypsin-ethylenediaminetetraacetic acid (0.25%) solution (25200056) WGA, AF-conjugated phalloidin, AF-conjugated secondary antibodies, and LAMP-1 antibody (MA5-29385) were purchased from Thermo Fisher Scientific. Primary antibodies for EEA-1 (3288S) and Rab7 (9367S) were purchased from Cell Signaling Technology. ONE-Glo Luciferase Assay System (E6110) was purchased from Promega Corporation. EasySep Direct Human T Cell Isolation Kit (19661), Lymphoprep, and Human Recombinant IL-2 (78145) were obtained from StemCell Technologies. PE antihuman CD19 (302208), BV 785 antihuman CD14 (301840), BV 510 antihuman CD3 (344828), and pacific blue antihuman HLA-DR (307633) antibodies were purchased from Biolegend. AF488 antihuman CD56 antibody was purchased from BD Biosciences. Firefly luciferase mRNA was purchased from Messenger Bio (Australia).

Synthesis of BG_{EDA} NPs, PG_{EDA} NPs, and $Dextran_{EDA}$ NPs. Glycogen (100 mg, corresponding to 0.6 mmol of glucose monomers) was dissolved in acetate buffer (5 mL, 0.8 M, pH 5.5). To achieve DS of 6, 10, and 20%, sodium periodate (6.6, 13, or 26 mg, respectively) was added, and the solutions were stirred for 2 h in the dark. Then, EDA (10.3, 20, or 40 μL, respectively) and sodium cyanoborohydride (19.4, 39, or 77 mg, respectively) were added. The pH was monitored and adjusted to 5.5 using 5 M HCl. The solution was stirred for 24 h in the dark. The final product was purified by dialysis (tube size 14 kDa) against sodium chloride (150 mM) for 1 day and against Milli-Q water for 5 days. Dextran (110 kDa) was modified by EDA (5%) using a similar protocol.

Loading and Release of RV from Glycogen NPs. The loading of RV into the glycogen NPs was performed as follows: glycogen NPs (3 mg) were first dissolved in DMSO (10 μL), followed by the addition of PBS (500 μL) and an aliquot (10 μL, 1 mg mL^{-1}) of RV dissolved in DMSO. The resulting solution was kept under stirring for 30 min. The loading capacity of the NP systems was evaluated by using spin columns (100 kDa) to filter the unloaded RV at 3000 rpm for 5 min. The pass-through solution was collected and analyzed using UV−vis spectroscopy (SPECORD 250 PLUS instrument) to estimate

https://doi.org/10.1021/acsnano.4c09156
ACS Nano 2024, 18, 28910−28923

the concentration of RV; a quartz cuvette (0.2 cm × 1 cm) with a path length of 1 cm was used. The slits were set to 4 nm. A solution containing only RV at the same concentration was used as control. The loading percentage was calculated using eq 1, as follows

$$\% \text{ loading} = \left(1 - \frac{\text{Abs NPs}}{\text{Abs ctrl}}\right) \times 100\% \quad (1)$$

where Abs NPs is the absorbance of the filtered solutions and Abs ctrl is the absorbance of the initial RV solution. The release of RV was also evaluated by UV−vis spectroscopy after spinning the samples with 100 and 30 kDa spin columns (3000 rpm, 5 min). A pure RV solution was used as control. The drug release from the glycogen NPs was assessed both in PBS (pH 7.4) and in the presence of 10% FBS.

Labeling of Samples with AF647 Dye. A known amount (2 mg) of BG NPs, PG NPs, BG_{EDA} NPs, or PG_{EDA} NPs was dissolved in 100 mM bicarbonate buffer (0.5 mL, pH 9.2). Next, an aliquot (20 or 40 μL for BG NPs and PG NPs) of 1 mg mL^{-1} AF647 dye dissolved in DMSO was added. The solution was stirred for 25 h. A further purification step was performed to remove excess dye adsorbed onto the NP surface by dialysis in sodium chloride (150 mM) using a 14 kDa tube for 1 day and against Milli-Q water for another 2 days to remove the salt.

^{1}H NMR Spectroscopy. ^{1}H NMR spectra of aqueous solutions of BG_{EDA} NPs and PG_{EDA} NPs (1 mg mL^{-1}) were recorded on a 600 MHz Bruker Avance III at 40 °C in H_2O and 10% D_2O. The data were processed using MestReNova software.

Degradation of Samples by α-Amylase and β-Amylase. The rate of degradation of the glycogen NPs by α-amylase and β-amylase was determined using the Somogyi−Nelson assay. The NPs (200 μL, 1 mg mL^{-1}) were first dissolved in PBS (10 mM, pH 7.4) and incubated at 37 °C with α-amylase (0.1 U mL^{-1}) or β-amylase (1 U mL^{-1}) for 3 h. For the assay, copper−carbonate−tartrate reagent was prepared. This first consisted of the preparation of stock I (sodium potassium tartrate tetrahydrate (1.2 g), sodium carbonate (2.4 g), sodium bicarbonate (1.6 g), and sodium sulfate (14.4 g) in Milli-Q water (80 mL)) and stock II (copper sulfate pentahydrate (0.4 g) and sodium sulfate (3.6 g) dissolved in Milli-Q water (20 mL)). The working reagent was then prepared by mixing 4 parts of stock I with 1 part of stock II. The arsenomolybdate color reagent was prepared by dissolving ammonium molybdate (2.5 g) in water, followed by mixing with concentrated sulfuric acid (2.1 mL). The resulting solution was mixed with a solution of sodium arsenate dibasic pentahydrate (0.3 g) in Milli-Q water (2.5 mL). Aliquots (45 μL) of the glycogen NP solutions before and after treatment with amylases were mixed with the working reagent (45 μL) in a 1.5 mL Eppendorf and heated at 90 °C for 20 min under dark (covered with aluminum foil) using a thermomixer. Triplicates were transferred to a 96-well microplate (Costar 3596, Corning, MA, USA) after cooling to room temperature, then the color reagent (45 μL) was added to each well and mixed via pipetting and allowed to stand for 15 min before the measurement. The absorbance was recorded at 600 nm using an Infinite M200 microplate reader (Tecan, Switzerland). For reference, glucose (considered as degraded glycogen) solutions at varying concentrations were prepared, and the absorbance was determined under the same conditions.

Characterization of PG_{EDA} NPs and BG_{EDA} NPs by STORM. PG_{EDA} NPs and BG_{EDA} NPs labeled with AF647 (0.1 mg mL^{-1}) were dispersed in 10% FBS and then deposited on a glass slide. After 30 min of incubation at 25 °C, unbound NPs were washed off with freshly prepared standard imaging buffer containing cysteamine. STORM images were acquired using a Nikon N-STORM system equipped with a Nikon 100 × 1.4 NA oil immersion objective. The focus and the total internal reflection fluorescence imaging angle were adjusted to obtain a high signal-to-noise ratio. A 647 nm laser was used for excitation of the fluorophores. All time lapses were recorded within a region of 256 pixels × 256 pixels using an EMCCD camera. For each image, 3000 frames were acquired sequentially using full laser power. STORM images were first processed with the STORM module of the NIS Elements Nikon software, where drift correction was performed, and a list of particle localizations were obtained by Gaussian fitting of the fluorescence spots of blinking dyes. Blinking events that were detected in ≤5 consecutive frames were counted as single molecules, whereas events detected in >5 consecutive frames were discarded (maximum trace length 5). The list of localizations was exported as a txt. File and analyzed using a python clustering analysis script.

Cell Culturing. Human breast epithelial cancer cells MDA-MB-231 were purchased from the American Type Culture Collection (USA) and cultured in DMEM supplemented with 10% FBS and 1% penicillin−streptomycin at 37 °C and 5% CO_2. After reaching 80−90% confluency, cells were detached using trypsin-ethylenediaminetetraacetic acid and reseeded in the relevant culture dish. J-Lat Tat-GFP clone A2, a noninfectious cell line derived from human Jurkat T cells that were infected with a single copy of HIV-1 provirus engineered to express GFP upon activation (from NIH AIDS Reagent Program) were cultured in suspension in RPMI medium supplemented with 10% FBS, 1% glutamine, and 1% penicillin−streptomycin at 37 °C and 5% CO_2. PBMCs were isolated from buffy coat by density gradient centrifugation in Lymphoprep medium, according to manufacturer's instructions, and used immediately for cell association studies. Human primary T cells were isolated from buffy coat using the EasySep Direct Human T Cell Isolation Kit, according to the manufacturer's protocol. After isolation, cells at a seeding density of 1 × 10^6 cells mL^{-1} were cultured in ImmunoCult Cell Culture medium supplemented with 10 ng mL^{-1} interleukin-2 (IL-2). All experiments were done under the human ethics application approval 2023-27294-42014-3 entitled "Investigation of the interaction between NPs and immune system cells".

Cell Association Studies Using Flow Cytometry. For the cell association studies, J-Lat A2 cells, human primary T cells, PBMCs, and MDA-MB-231 cells were exposed to glycogen NPs labeled with AF647 for 2, 5, and 24 h. In the case of MDA-MB-231 cells, 60000 cells per well were seeded onto a 24-multiwell plate 24 h before the addition of the glycogen NPs. Subsequently, the culture medium was replaced with fresh medium containing NPs at a final concentration of 0.5 mg mL^{-1} and the cells were incubated at 37 °C. At designated time points, the cells were washed three times with DPBS, detached using trypsin, and after centrifugation washed twice before proceeding with flow cytometry measurements. For J-Lat A2 and primary T cells, 75000 cells were seeded per well in a round-bottom 96-multiwell plate before the addition of NPs at a final dosage of 0.5 mg mL^{-1}. After defined incubation periods, the cells were collected by centrifugation, washed three times, and subjected to flow cytometry measurements. Measurements were conducted using a BD Accuri C6 Plus or a BD FACSCanto II cytometer. For PBMCs, cells were plated in 24-well plates at a seeding density of 1 × 10^6 cells per well and equilibrated for 30 min at 37 °C. Then, PBMCs were treated with 5 mg mL^{-1} NPs. At the specified time points, cells were washed twice with flow cytometry staining buffer (0.5% BSA and 2 mM EDTA in DPBS). The cells were then stained on ice for 30 min using titrated concentrations of CD19 (PE), CD56 (AF488), CD14 (BV 785), CD3 (BV 510), and HLA-DR (pacific blue) antibodies. Cells were washed twice with cold DPBS, fixed with 4% PFA for 10 min, washed again twice with cold DPBS and subjected to flow cytometry (LSR Fortessa). All data were analyzed using FlowJo v.10 (BD Biosciences).

Intracellular Trafficking and Colocalization Studies in Fixed Cells by Confocal Microscopy. For the intracellular trafficking studies, approximately 40000 MDA-MB-231 cells were seeded on 8-well Lab-Tek chamber slides, followed by the addition of the culture medium (0.5 mL) and incubation overnight. The cells were then incubated with glycogen NPs (1 mg mL^{-1}) in DMEM supplemented with 10% FBS for 2, 5, and 24 h with a washing step with 1× PBS after the first 2 h. The cells were fixed for 10 min in 4% PFA. Next, samples were permeabilized with 0.1% Triton X-100 for 10 min at room temperature. After two washing steps with DPBS, blocking was performed using 2.5% BSA in DPBS for 30 min at room temperature. Primary antibodies (1:200, v/v) for EEA-1, Rab7, and LAMP-1 were incubated overnight at 4 °C and then washed with DPBS twice prior to incubation with AF-conjugated secondary antibodies (1:500, v/v).

https://doi.org/10.1021/acsnano.4c09156
ACS Nano 2024, 18, 28910−28923

Two additional washes were performed before the cell nuclei were stained with Hoechst 33342 fluorescent dye and the cell membrane was stained with WGA. Once labeling was completed, the cells were washed twice with DPBS and kept in clean DPBS at 4 °C until imaged. The cells were imaged with a Nikon A1R confocal microscope. For the colocalization studies, PCCs were obtained using ImageJ software.

For J-Lat A2 cells, 75000 cells were seeded per well in a round-bottom 96-multiwell plate before the addition of NPs at a final dosage of 1 mg mL^{-1}. The cells exposed to the NPs were incubated at 37 °C for 5 and 24 h, with a washing step at 5 h. After the incubation period, the cells were collected by centrifugation, washed three times, and fixed for 10 min in 4% PFA. Subsequent permeabilization, blocking, and immunocytochemistry procedures were performed similarly to those described for MDA-MB-231 cells.

Cell Viability Assay. The viability of MDA-MB-231 and J-Lat A2 cells was determined by Alamar blue assay as described by the manufacturer. After incubation with the NPs and/or free drug, the culture medium was removed and replaced with fresh medium containing 10% alamar blue reagent. The cells were incubated at 37 °C for 4 h, and the absorbance was measured at 570 nm with 600 nm reference. The results are represented as percentage of live cells normalized to the untreated control.

NPs Internalization Assessed by Imaging Flow Cytometry. For the cell internalization studies, J-Lat A2 cells were exposed to glycogen NPs labeled with AF647 for 24 h. A total of 200,000 cells were seeded per well in a round-bottom 96-multiwell plate before the addition of NPs at a final dosage of 1 mg mL^{-1}. After 24 h, the cells were collected by centrifugation, washed three times with DPBS, fixed in PFA 4%, washed again, and resuspended in DPBS (30 μL). All measurements were conducted using an Amnis ImageStream X MkII imaging flow cytometer (ISX) and the data analyzed with IDEAS software using the internalization wizard and the workflow reported in Figure S5 to exclude dead cells, duplets, and agglomerated AF647 signal.

Preparation of NPs-mRNA Complexes and Characterization by Gel Retardation Assay. The complexation of the glycogen NPs and mRNA-Luc was performed at a ratio of 75 μg NPs:1 μg mRNA-Luc in Opti-MEM. mRNA alone was used as a control. An aliquot (20 μL) of each sample (mRNA, PG_{EDA}-mRNA-Luc, and BG_{EDA}-mRNA-Luc) was loaded to an agarose gel (1% low electroendosmotic agarose), and electrophoresis was performed in tris/borate/EDTA buffer for 15 min at 150 V, followed by 30 min at 90 V. The gel was analyzed and images were acquired using a BIO-RAD Gel Doc XR^+ system.

Delivery of mRNA-Luc to J-Lat A2 and Primary T Cells Using BG_{EDA} NPs and PG_{EDA} NPs. For the transfection experiments, 75,000 J-Lat A2 cells were seeded per well in a round-bottom 96-multiwell plate before the addition of NPs (final dosage of 0.5 mg mL^{-1}) and mRNA encoding luciferase per well (1 μg, in a total volume of 150 μL). Lipofectamine (RNAiMAX) was used as a positive control for the transfection efficiency according to the supplier's protocol and 1 μg of mRNA encoding luciferase per well in a total volume of 150 μL. After incubation for 4 h at 37 °C and 5% CO_2, using Opti-MEM, the growth medium was replaced with RPMI containing 10% FBS, and the cells were incubated further for 20 h. After the 24 h incubation period, mRNA transfection efficiency was estimated using the ONE-Glo EX Luciferase Assay System according to the manufacturer's procedure.

Statistical Analysis. All results are shown as mean ± standard deviation. The statistical significance and p values were determined with GraphPad Prism 8 using the tests specified in the figure captions.

Image Analysis. All images acquired by confocal microscopy were analyzed using ImageJ. For the 3D reconstruction of J-Lat A2 cells, IMARIS 9.6.1 was used.

Minimum Information Reporting in Bio–Nano Experimental Literature (MIRIBEL). The studies conducted herein, including material characterization, biological characterization, and experimental details, conform to the MIRIBEL reporting standard for bio–nano research,[45] and we include a companion checklist of these components in the Supporting Information.

ASSOCIATED CONTENT

Supporting Information

The Supporting Information is available free of charge at https://pubs.acs.org/doi/10.1021/acsnano.4c09156.

Characterization of glycogen NPs; ^1H NMR spectra of BG_{EDA} and PG_{EDA} NPs; J-Lat A2 cell viability data after incubation with glycogen NPs; flow cytometry analysis of association of glycogen NPs with J-LAT A2 cells; RV toxicity against J-Lat A2 cells; GFP expression of J-LAT A2 cells after treatment with glycogen NPs loaded with RV; confocal images of intracellular trafficking of BG_{EDA} NPs and PG_{EDA} NPs in J-LAT A2 cells; imaging flow cytometer analysis of NP internalization; gel retardation assay for confirming mRNA binding to glycogen NPs; flow cytometry analysis of association of glycogen with PBMCs; mRNA-Luc transfection control, in J-Lat A2 cells and human primary T cells, using Lipofectamine (PDF)

AUTHOR INFORMATION

Corresponding Authors

Frank Caruso − *Department of Chemical Engineering, The University of Melbourne, Parkville 3010 Victoria, Australia;* orcid.org/0000-0002-0197-497X; Email: fcaruso@unimelb.edu.au

Francesca Cavalieri − *School of Science, RMIT University, Melbourne 3000 Victoria, Australia; Dipartimento di Scienze e Tecnologie Chimiche, Universita di Roma "Tor Vergata", 00133 Rome, Italy;* orcid.org/0000-0001-5391-5069; Email: francesca.cavalieri@rmit.edu.au

Authors

Soraia Fernandes − *Department of Chemical Engineering, The University of Melbourne, Parkville 3010 Victoria, Australia; International Clinical Research Centre, 656 91 Brno, Czech Republic*

Miriam Quattrociocchi − *Department of Chemical Engineering, The University of Melbourne, Parkville 3010 Victoria, Australia*

Marco Cassani − *Department of Chemical Engineering, The University of Melbourne, Parkville 3010 Victoria, Australia; International Clinical Research Centre, 656 91 Brno, Czech Republic*

Giulio Savazzi − *Department of Chemical Engineering, The University of Melbourne, Parkville 3010 Victoria, Australia*

Darryl Johnson − *Materials Characterization and Fabrication Platform, Department of Chemical Engineering, The University of Melbourne, Parkville 3010 Victoria, Australia;* orcid.org/0000-0003-3205-0371

Giancarlo Forte − *International Clinical Research Centre, 656 91 Brno, Czech Republic; School of Cardiovascular and Metabolic Medicine & Sciences, King's College London, London SE5 9NU, U.K.*

Complete contact information is available at: https://pubs.acs.org/10.1021/acsnano.4c09156

Author Contributions

The manuscript was written through contributions of all authors. All authors have given approval to the final version of the manuscript.

Notes

The authors declare no competing financial interest.

ACKNOWLEDGMENTS

F.C. acknowledges the award of an RMIT Vice Chancellor Senior Research Fellowship. This work was supported by the Australian Research Council under a Discovery Project scheme (F.C.; DP210101792) and funded in part by the National Health and Medical Research Council (GNT2016732, F.Caruso). For the purposes of open access, the author has applied a CC BY public copyright license to any Author Accepted Manuscript version arising from this submission. This work received funding from the European Union's Horizon 2020 research and innovation program under the Marie Skłodowska-Curie grant agreement no. 872233 ("PEPSA-MATE"). M.C. acknowledges funding from a Marie Curie H2020-MSCA-IF-2020 MSCA-IF-GF grant agreement no. 101031744 ("MecHA-Nano"). G.F. acknowledges the King's BHF Centre for Excellence Award (RE/18/2/34213). This work was performed in part at the Materials Characterization and Fabrication Platform (MCFP). The following reagent was obtained through the NIH AIDS Reagent Program, Division of AIDS, NIAID, NIH: J-Lat Tat-GFP Cells (clone A2) from Dr. Eric Verdin. The authors acknowledge Smita Agarwal, Brendan Dyett and Haleh Mahmoudinoodezh for assisting with NMR spectra, clustering analysis script and synthesis of samples. The table of contents graphic was partially created with BioRender.com.

REFERENCES

(1) Besford, Q. A.; Cavalieri, F.; Caruso, F. Glycogen as a Building Block for Advanced Biological Materials. *Adv. Mater.* **2020**, *32*, No. e1904625.

(2) Besford, Q. A. The Sweetest Polymer Nanoparticles: Opportunities Ahead for Glycogen in Nanomedicine. *Soft Matter* **2024**, *20*, 3577−3584.

(3) Odeniyi, M. A.; Omoteso, O. A.; Adepoju, A. O.; Jaiyeoba, K. T. Starch Nanoparticles in Drug Delivery: A Review. *Polym. Med.* **2019**, *48*, 41−45.

(4) Troncoso, O. P.; Torres, F. G. Non-Conventional Starch Nanoparticles for Drug Delivery Applications. *Med. Devices Sens.* **2020**, *3*, No. e10111.

(5) Wang, H.; Dai, T.; Zhou, S.; Huang, X.; Li, S.; Sun, K.; Zhou, G.; Dou, H. Self-Assembly Assisted Fabrication of Dextran-Based Nanohydrogels with Reduction-Cleavable Junctions for Applications as Efficient Drug Delivery Systems. *Sci. Rep.* **2017**, *7*, 40011.

(6) Hu, Q.; Lu, Y.; Luo, Y. Recent Advances in Dextran-Based Drug Delivery Systems: From Fabrication Strategies to Applications. *Carbohydr. Polym.* **2021**, *264*, 117999.

(7) Sun, B.; Zhang, M.; Shen, J.; He, Z.; Fatehi, P.; Ni, Y. Applications of Cellulose-Based Materials in Sustained Drug Delivery Systems. *Curr. Med. Chem.* **2019**, *26*, 2485−2501.

(8) Ai, Y.; Lin, Z.; Zhao, W.; Cui, M.; Qi, W.; Huang, R.; Su, R. Nanocellulose-Based Hydrogels for Drug Delivery. *J. Mater. Chem. B* **2023**, *11*, 7004−7023.

(9) Farasati Far, B.; Omrani, M.; Naimi Jamal, M. R.; Javanshir, S. Multi-Responsive Chitosan-Based Hydrogels for Controlled Release of Vincristine. *Commun. Chem.* **2023**, *6*, 28.

(10) Sultan, M. H.; Moni, S. S.; Madkhali, O. A.; Bakkari, M. A.; Alshahrani, S.; Alqahtani, S. S.; Alhakamy, N. A.; Mohan, S.; Ghazwani, M.; Bukhary, H. A.; Almoshari, Y.; Salawi, A.; Alshamrani, M. Characterization of Cisplatin-Loaded Chitosan Nanoparticles and Rituximab-Linked Surfaces as Target-Specific Injectable Nano-Formulations for Combating Cancer. *Sci. Rep.* **2022**, *12*, 468.

(11) Jia, Y.; Chen, S.; Wang, C.; Sun, T.; Yang, L. Hyaluronic Acid-Based Nano Drug Delivery Systems for Breast Cancer Treatment: Recent Advances. *Front. Bioeng. Biotechnol.* **2022**, *10*, 990145.

(12) Lei, C.; Liu, X.-R.; Chen, Q.-B.; Li, Y.; Zhou, J.-L.; Zhou, L.-Y.; Zou, T. Hyaluronic Acid and Albumin Based Nanoparticles for Drug Delivery. *J. Controlled Release* **2021**, *331*, 416−433.

(13) Cadete, A.; Olivera, A.; Besev, M.; Dhal, P. K.; Gonçalves, L.; Almeida, A. J.; Bastiat, G.; Benoit, J.-P.; de la Fuente, M.; Garcia-Fuentes, M.; Alonso, M. J.; Torres, D. Self-Assembled Hyaluronan Nanocapsules for the Intracellular Delivery of Anticancer Drugs. *Sci. Rep.* **2019**, *9*, 11565.

(14) Baek, M.-J.; Nguyen, D.-T.; Kim, D.; Yoo, S.-Y.; Lee, S. M.; Lee, J.-Y.; Kim, D.-D. Tailoring Renal-Clearable Zwitterionic Cyclodextrin for Colorectal Cancer-Selective Drug Delivery. *Nat. Nanotechnol.* **2023**, *18*, 945−956.

(15) Doan, V. T. H.; Lee, J. H.; Takahashi, R.; Nguyen, P. T. M.; Nguyen, V. A. T.; Pham, H. T. T.; Fujii, S.; Sakurai, K. Cyclodextrin-Based Nanoparticles Encapsulating α-Mangostin and Their Drug Release Behavior: Potential Carriers of α-Mangostin for Cancer Therapy. *Polym. J.* **2020**, *52*, 457−466.

(16) Bai, H.; Wang, J.; Phan, C. U.; Chen, Q.; Hu, X.; Shao, G.; Zhou, J.; Lai, L.; Tang, G. Cyclodextrin-Based Host-Guest Complexes Loaded with Regorafenib for Colorectal Cancer Treatment. *Nat. Commun.* **2021**, *12*, 759.

(17) Rodriguez-Rosales, R. J.; Yao, Y. Phytoglycogen, a Natural Dendrimer-Like Glucan, Improves the Soluble Amount and Caco-2 Monolayer Permeation of Curcumin and Enhances Its Efficacy to Reduce HeLa Cell Viability. *Food Hydrocolloids* **2020**, *100*, 105442.

(18) Chen, H.; Yao, Y. Phytoglycogen Improves the Water Solubility and Caco-2 Monolayer Permeation of Quercetin. *Food Chem.* **2017**, *221*, 248−257.

(19) Chen, H.; Yao, Y. Phytoglycogen to Increase Lutein Solubility and Its Permeation through Caco-2 Monolayer. *Food Res. Int.* **2017**, *97*, 258−264.

(20) Zhou, J.; Han, Y.; Yang, Y.; Zhang, L.; Wang, H.; Shen, Y.; Lai, J.; Chen, J. Phospholipid-Decorated Glycogen Nanoparticles for Stimuli-Responsive Drug Release and Synergetic Chemophotothermal Therapy of Hepatocellular Carcinoma. *ACS Appl. Mater. Interfaces* **2020**, *12*, 23311−23322.

(21) Han, Y.; Hu, B.; Wang, M.; Yang, Y.; Zhang, L.; Zhou, J.; Chen, J. pH-Sensitive Tumor-Targeted Hyperbranched System Based on Glycogen Nanoparticles for Liver Cancer Therapy. *Appl. Mater. Today* **2020**, *18*, 100521.

(22) Li, X.; Chen, X.-X.; Xu, Y.; Xu, X.-B.; Wu, W.-F.; Zhao, Q.; Hu, J.-N. Construction of Glycogen-Based Nanoparticles Loaded with Resveratrol for the Alleviation of High-Fat Diet-Induced Non-alcoholic Fatty Liver Disease. *Biomacromolecules* **2022**, *23*, 409−423.

(23) Wojnilowicz, M.; Besford, Q. A.; Wu, Y. L.; Loh, X. J.; Braunger, J. A.; Glab, A.; Cortez-Jugo, C.; Caruso, F.; Cavalieri, F. Glycogen-Nucleic Acid Constructs for Gene Silencing in Multicellular Tumor Spheroids. *Biomaterials* **2018**, *176*, 34−49.

(24) Liu, Z.; Gong, H.; Zeng, R.; Liang, X.; Zhang, L.-M.; Yang, L.; Lan, Y. Efficient Delivery of NF-κB siRNA to Human Retinal Pigment Epithelial Cells with Hyperbranched Cationic Polysaccharide Derivative-Based Nanoparticles. *Int. J. Nanomed.* **2015**, *10*, 2735−2749.

(25) Engelberth, S. A.; Hempel, N.; Bergkvist, M. Chemically Modified Dendritic Starch: A Novel Nanomaterial for siRNA Delivery. *Bioconjugate Chem.* **2015**, *26*, 1766−1774.

(26) Liang, X.; Ren, X.; Liu, Z.; Liu, Y.; Wang, J.; Wang, J.; Zhang, L.-M.; Deng, D. Y. B.; Quan, D.; Yang, L. An Efficient Nonviral Gene-Delivery Vector Based on Hyperbranched Cationic Glycogen Derivatives. *Int. J. Nanomed.* **2014**, *9*, 419−435.

(27) Xu, R.; Bhangu, S. K.; Sourris, K. C.; Vanni, D.; Sani, M.-A.; Karas, J. A.; Alt, K.; Niego, B.; Ale, A.; Besford, Q. A.; Dyett, B.;

https://doi.org/10.1021/acsnano.4c09156
ACS Nano 2024, 18, 28910−28923

Patrick, J.; Carmichael, I.; Shaw, J. E.; Caruso, F.; Cooper, M. E.; Hagemeyer, C. E.; Cavalieri, F. An Engineered Nanosugar Enables Rapid and Sustained Glucose-Responsive Insulin Delivery in Diabetic Mice. *Adv. Mater.* **2023**, *35*, 2210392.
(28) Radziwon, A.; Bhangu, S. K.; Fernandes, S.; Cortez-Jugo, C.; De Rose, R.; Dyett, B.; Wojnilowicz, M.; Laznickova, P.; Fric, J.; Forte, G.; Caruso, F.; Cavalieri, F. Triggering the Nanophase Separation of Albumin through Multivalent Binding to Glycogen for Drug Delivery in 2D and 3D Multicellular Constructs. *Nanoscale* **2022**, *14*, 3452−3466.
(29) Wojnilowicz, M.; Glab, A.; Bertucci, A.; Caruso, F.; Cavalieri, F. Super-resolution Imaging of Proton Sponge-Triggered Rupture of Endosomes and Cytosolic Release of Small Interfering RNA. *ACS Nano* **2019**, *13*, 187−202.
(30) Bhangu, S. K.; Mummolo, L.; Fernandes, S.; Amodio, A.; Radziwon, A.; Dyett, B.; Savioli, M.; Mantri, N.; Cortez-Jugo, C.; Caruso, F.; Cavalieri, F. Tracking the Endosomal Escape of Nanoparticles in Live Cells Using a Triplex-Forming Oligonucleotide. *Adv. Funct. Mater.* **2024**, *34*, 2311240.
(31) Olden, B. R.; Cheng, E.; Cheng, Y.; Pun, S. H. Identifying Key Barriers in Cationic Polymer Gene Delivery to Human T Cells. *Biomater. Sci.* **2019**, *7*, 789−797.
(32) Cevaal, P. M.; Ali, A.; Czuba-Wojnilowicz, E.; Symons, J.; Lewin, S. R.; Cortez-Jugo, C.; Caruso, F. *In Vivo* T Cell-Targeting Nanoparticle Drug Delivery Systems: Considerations for Rational Design. *ACS Nano* **2021**, *15*, 3736−3753.
(33) Symons, J.; Chopra, A.; Malatinkova, E.; De Spiegelaere, W.; Leary, S.; Cooper, D.; Abana, C. O.; Rhodes, A.; Rezaei, S. D.; Vandekerckhove, L.; Mallal, S.; Lewin, S. R.; Cameron, P. U. HIV Integration Sites in Latently Infected Cell Lines: Evidence of Ongoing Replication. *Retrovirology* **2017**, *14*, 2.
(34) Jordan, A.; Bisgrove, D.; Verdin, E. HIV Reproducibly Establishes a Latent Infection After Acute Infection of T Cells In Vitro. *EMBO J.* **2003**, *22*, 1868−1877.
(35) Jordan, A.; Defechereux, P.; Verdin, E. The Site of HIV-1 Integration in the Human Genome Determines Basal Transcriptional Activity and Response to Tat Transactivation. *EMBO J.* **2001**, *20*, 1726−1738.
(36) Aggarwal, B. B.; Bhardwaj, A.; Aggarwal, R. S.; Seeram, N. P.; Shishodia, S.; Takada, Y. Role of Resveratrol in Prevention and Therapy of Cancer: Preclinical and Clinical Studies. *Anticancer Res.* **2004**, *24*, 2783−2840.
(37) Zeng, X.; Pan, X.; Xu, X.; Lin, J.; Que, F.; Tian, Y.; Li, L.; Liu, S. Resveratrol Reactivates Latent HIV through Increasing Histone Acetylation and Activating Heat Shock Factor 1. *J. Agric. Food Chem.* **2017**, *65*, 4384−4394.
(38) Zhao, N.; Qi, J.; Zeng, Z.; Parekh, P.; Chang, C. C.; Tung, C. H.; Zu, Y. Transfecting the Hard-to-Transfect Lymphoma/Leukemia Cells Using a Simple Cationic Polymer Nanocomplex. *J. Controlled Release* **2012**, *159*, 104−110.
(39) Favretto, M. E.; Wallbrecher, R.; Schmidt, S.; van de Putte, R.; Brock, R. Glycosaminoglycans in the Cellular Uptake of Drug Delivery Vectors - Bystanders or Active Players? *J. Controlled Release* **2014**, *180*, 81−90.
(40) Wojnilowicz, M.; Laznickova, P.; Ju, Y.; Ang, C. S.; Tidu, F.; Bendickova, K.; Forte, G.; Plebanski, M.; Caruso, F.; Cavalieri, F.; Fric, J. Influence of Protein Corona on the Interaction of Glycogen-siRNA Constructs with *Ex Vivo* Human Blood Immune Cells. *Biomater. Adv.* **2022**, *140*, 213083.
(41) Wong, L. M.; Li, D.; Tang, Y.; Méndez-Lagares, G.; Thompson, G. R., 3rd.; Hartigan-O'Connor, D. J.; Dandekar, S.; Jiang, G. Human Immunodeficiency Virus-1 Latency Reversal *Via* the Induction of Early Growth Response Protein 1 to Bypass Protein Kinase C Agonist-Associated Immune Activation. *Front. Microbiol.* **2022**, *13*, 836831.
(42) Pan, X.-Y.; Zhao, W.; Zeng, X.-Y.; Lin, J.; Li, M.-M.; Shen, X.-T.; Liu, S.-W. Heat Shock Factor 1 Mediates Latent HIV Reactivation. *Sci. Rep.* **2016**, *6*, 26294.
(43) Paramasivam, P.; Franke, C.; Stöter, M.; Höijer, A.; Bartesaghi, S.; Sabirsh, A.; Lindfors, L.; Arteta, M. Y.; Dahlén, A.; Bak, A.; Andersson, S.; Kalaidzidis, Y.; Bickle, M.; Zerial, M. Endosomal Escape of Delivered mRNA from Endosomal Recycling Tubules Visualized at the Nanoscale. *J. Cell Biol.* **2022**, *221*, No. e202110137.
(44) Billingsley, M. M.; Singh, N.; Ravikumar, P.; Zhang, R.; June, C. H.; Mitchell, M. J. Ionizable Lipid Nanoparticle-Mediated mRNA Delivery for Human CAR T Cell Engineering. *Nano Lett.* **2020**, *20*, 1578−1589.
(45) Faria, M.; Björnmalm, M.; Thurecht, K. J.; Kent, S. J.; Parton, R. G.; Kavallaris, M.; Johnston, A. P. R.; Gooding, J. J.; Corrie, S. R.; Boyd, B. J.; Thordarson, P.; Whittaker, A. K.; Stevens, M. M.; Prestidge, C. A.; Porter, C. J. H.; Parak, W. J.; Davis, T. P.; Crampin, E. J.; Caruso, F. Minimum Information Reporting in Bio−Nano Experimental Literature. *Nat. Nanotechnol.* **2018**, *13*, 777−785.

https://doi.org/10.1021/acsnano.4c09156
ACS Nano 2024, 18, 28910−28923